Exploring novel therapeutics for lung cancer with drug repositioning.

ドラッグリポジショニングを活用した肺がんに対する新規治療薬の探索

Joint Graduate School of Veterinary Medicine

Yamaguchi University

Kosuke Ochi

March 2023

TABLE OF CONTENTS

LIST OF PUBLICATIONS ····· 1

GENERAL INTRODUCTION ····· 2

CHAPTER 1: Overcoming epithelial-mesenchymal transition-mediated drug resistance with monensin-based combined therapy in non-small cell lung cancer

1. Abstract ····· 5
2. Introduction ····· 6
3. Materials and methods ····· 8
4. Results ····· 11
5. Discussion ····· 16
6. Tables and Figures ····· 21
7. References ····· 30

CHAPTER 2: Drug repositioning of tranilast to sensitize a cancer therapy by targeting cancer-associated fibroblast

1. Abstract ····· 33
2. Introduction ····· 34

3. Materials and methods ……37

4. Results ……42

5. Discussion ……47

6. Figures ……51

7. References ……65

GENERAL CONCLUSION ……68

LIST OF ORIGINAL PUBLICATIONS

Parts of this thesis have been published as:

1. Ochi, K., Suzawa, K., Tomida, S., Shien, K., Takano, J., Miyauchi, S., Takeda, T., Miura, A., Araki, K., Nakata, K., Yamamoto, H., Okazaki, M., Sugimoto, S., Shien, T., Yamane, M., Azuma, K., Okamoto, Y., Toyooka, S. 2020. Overcoming epithelial-mesenchymal transition-mediated drug resistance with monensin-based combined therapy in non-small cell lung cancer. *Biochem Biophys Res Commun.* 27;529(3):760-765.

2. Ochi, K., Suzawa, K., Thu YM, Takatsu, F., Tsudaka, S., Zhu, Y., Nakata, K., Takeda, T., Shien, K., Yamamoto, H., Okazaki, M., Sugimoto, S., Shien, T., Okamoto, Y., Tomida, S., Toyooka, S. 2022. Drug repositioning of tranilast to sensitize a cancer therapy by targeting cancer-associated fibroblast. *Cancer Sci.* 113(10):3428-3436.

GENERAL INTRODUCTION

Lung cancer is the leading cause of cancer death worldwide. Significant advances have been made in the treatment of non-small cell lung cancer (NSCLC) with the development of drugs targeting oncogenic driver mutations or immune checkpoint molecules, which have enabled precision medicine. However, while most molecular-targeted therapies initially show significant effect, acquired resistance to the drugs eventually develops; and efforts are being made to develop complementary therapies to maximize the effects of the targeted therapies or overcome the acquired drug resistance. A variety of resistance mechanisms to anticancer drugs, especially to molecular-targeted drugs, have been elucidated, including second-site mutations in the kinase domain, bypass signaling pathway activation, copy number changes, and histologic transformation, although many questions still remain.

The epithelial-mesenchymal transition (EMT) is an important mechanism of drug resistance acquisition. The EMT is a phenotypic conversion of epithelial features into mesenchymal features: a decrease in intracellular adhesion and cell polarity, and an increase in matrix remodeling and motility. These changes confer the tumor metastatic behaviors of cancer cell invasion and migration. Several key

signaling pathways, including transforming growth factor-β (TGF-β) and so on. The EMT is also known to be involved in resistance to a variety of therapeutic modalities, including chemotherapy with cytotoxic drugs or molecularly targeted drugs, as well as radiation therapy in diverse cancer types. The mechanism of this EMT-mediated drug resistance has been studied for decades; so far, EMT-driven cancer stem cell (CSC)-like properties, such as an increase in drug efflux and anti-apoptotic effects, have received attention for their pivotal roles in cancer drug resistance.

On the other hand, drug resistance due to CAFs has also recently received attention. Cancer-related fibroblasts (CAFs) are one of the major components of the tumor stroma and contribute significantly to the tumor microenvironment. It has been shown that CAFs release several cytokines, such as interleukin-6 (IL-6), TGF-β and epidermal growth factor (EGF), which activate multiple signaling pathways in cancer cells to promote tumor cell proliferation, invasion, metastasis and chemoresistance. It has been reported that activation of the IL-6/STAT3 signaling pathway in NSCLC cells by substances secreted by CAFs is a critical contributor to CAF-mediated drug resistance. Therefore, CAF-targeted therapy is gaining attention as one of the complementary treatment strategies for cancer.

Drug repositioning (or repurposing/reprofiling) is the process of finding new therapeutic indications for existing drugs. This approach represents an increasingly promising, cost-effective alternative strategy for accelerating the development of treatments for diseases, since previous development efforts and preclinical and clinical data, especially safety profiles, are usually available. Several drugs have been successfully repositioned for new indications, with two of the most notable examples being sildenafil and thalidomide.

In this study, the effect of monensin on the prevention of drug resistance was examined in chapter 1. In chapter 2, we assessed the inhibitory effect of tranilast to overcome Cancer-associated fibroblast (CAF)-mediated acquisition of drug resistance in cancer treatment.

CHAPTER 1

Overcoming epithelial-mesenchymal transition-mediated drug resistance with monensin-based combined therapy in non-small cell lung cancer

Abstract

Background: The epithelial-mesenchymal transition (EMT) is a key process in tumor progression and metastasis and is also associated with drug resistance. Thus, controlling EMT status is a research of interest to conquer the malignant tumors.

Materials and methods: A drug repositioning analysis of transcriptomic data from a public cell line database identified monensin, a widely used in veterinary medicine, as a candidate EMT inhibitor that suppresses the conversion of the EMT phenotype. Using TGF-β-induced EMT cell line models, the effects of monensin on the EMT status and EMT-mediated drug resistance were assessed.

Results: TGF-β treatment induced EMT in non-small cell lung cancer (NSCLC) cell lines and the *EGFR*-mutant NSCLC cell lines with TGF-β-induced EMT acquired resistance to EGFR-tyrosine kinase inhibitor. The addition of monensin

effectively suppressed the TGF-β-induced-EMT conversion, and restored the growth inhibition and the induction of apoptosis by the EGFR-tyrosine kinase inhibitor.

Conclusion: Our data suggested that combined therapy with monensin might be a useful strategy for preventing EMT-mediated acquired drug resistance.

Introduction

The epithelial-mesenchymal transition (EMT) is a phenotypic conversion of epithelial features into mesenchymal features: a decrease in intracellular adhesion and cell polarity, and an increase in matrix remodeling and motility. These changes confer the tumor metastatic behaviors of cancer cell invasion and migration. Several key signaling pathways, including transforming growth factor-β (TGF-β), Wnt, Notch and Hedgehog, are involved in this process. Of these, TGF-β is considered to be a pivotal mediator of the EMT during physiological processes (1-3), and TGF-β treatment is a well-established method of inducing the EMT *in vitro* in cell line models (4). The EMT is also known to be involved in resistance to a variety of therapeutic modalities, including chemotherapy with

cytotoxic drugs or molecularly targeted drugs, as well as radiation therapy in diverse cancer types (2, 5). The mechanism of this EMT-mediated drug resistance has been studied for decades; so far, EMT-driven cancer stem cell (CSC)-like properties, such as an increase in drug efflux and anti-apoptotic effects, have received attention for their pivotal roles in cancer drug resistance (1, 2, 6, 7). The EMT is a promising target for novel therapeutic strategies targeting cancer progression and drug resistance; however, this approach is potentially challenging because the EMT is intricately regulated by numerous factors, such as extracellular matrix components, diverse signal pathways, soluble growth factors or cytokines, and microRNAs (1, 2, 8).

The process of finding new uses outside the scope of the original medical indications of existing drugs is known as drug repositioning. This approach represents an increasingly promising, cost-effective alternative strategy for accelerating the development of treatments for diseases, since previous development efforts and preclinical and clinical data, especially safety profiles, are usually available (9). Several drugs have been successfully repositioned for new indications, with two of the most notable examples being sildenafil and thalidomide (10).

In this study, we conducted an *in silico* drug repositioning analysis of transcriptomic data from a cell line database and identified monensin as a candidate EMT inhibitor capable of reversing the EMT phenotype. Monensin is a polyether ionophore that is widely used as an antibiotic in livestock animals (11). We then assessed the inhibitory effect of monensin on the EMT phenotype and its potential to overcome EMT-mediated drug resistance.

Materials and methods

Bioinformatics analysis

Comprehensive transcriptomic profiles of 28 NSCLC cell lines were obtained from the Cancer Cell Line Encyclopedia (CCLE) database (http://www.broadinstitute.org/ccle/). Gene set enrichment analysis (GSEA) was performed using GSEA_4.0.1 software and a database of gene sets obtained from Molecular Signatures Database v5.0 (https://www.gsea-msigdb.org/gsea/) (12). A Connectivity Map (C-MAP) analysis was performed using the tool described by Lamb and colleagues (13). We selected 164 probes that were positively correlated with the expression pattern of mir-200c and an additional 124 probes that were negatively correlated with the expression pattern of mir-200c in the

CCLE database; we then used the selected probes as queries in comparisons with the rank-ordered lists for each drug treatment in the C-MAP database. Since C-MAP analysis is only applicable for Affymetrix type probe IDs of HG-U133A Gene Chips, we transformed the probe IDs from HG-U133 plus2 Gene Chips in the CCLE database into HG-U133A based on gene symbol comparisons using the GPL96 file from GEO (http://www.ncbi.nlm.nih.gov/geo/). As a result, 87 of the 164 positive-correlated probes and 52 of the 124 negative-correlated probes were used for C-MAP analysis.

Cell culture and reagents

Two EGFR-mutant NSCLC cell lines: HCC827 (EGFR exon19del E746-A750), H1975 (EGFR L858R and T790M), one KRAS mutant NSCLC cell line, A549 (KRAS G12S) and one pancreatic cancer cell line, PANC-1 (KRAS G12D), were used in this study. All cell lines were purchased from the American Type Culture Collection (Manassas, VA, USA). These cell lines were cultured in Roswell Park Memorial Institute-1640 medium supplemented with 10% fetal bovine serum at 37 ºC in humidified incubator under 5% CO2 gas. Osimertinib, EGFR-tyrosine kinase inhibitor, was purchased from ChemScene (Monmouth Junction, NJ, USA)

and monensin was purchased from Cayman Chemical (Ann Arbor, MI, USA). TGF-β was purchased from Wako (Osaka, Japan).

Cell viability assay

The sensitivity to each drug was determined by a modified MTS assay. Cells were plated at a density of 3,000 cells per well in 96-well plates, and treated with the desired concentration of drugs. Cell viability was assayed after 96 hours of treatment using CellTiter 96 Aqueous bromide One Solution Reagent (Promega, Madison, WI, USA). For measurement of IC_{50} value, each condition was assayed in eight-replicate determinations in three independent experiments. Data was analyzed by non-linear regression using Graphpad Prism Ver. 6.0.3 (GraphPad Software, San Diego, CA).

Western blotting

Cells were treated with ethanol (Wako, Osaka, Japan) as a control, 2 ng/mL TGF-β and 100 nM monensin. The total cell lysate was extracted with lysis buffer, a mixture of RIPA buffer, phosphate inhibitor cocktails 2 and 3 (Sigma-Aldrich, St. Louis, MO, USA) and complete Mini Protease Inhibitor Cocktail (Roche,

Switzerland). Western blot analysis was performed by using the following primary antibodies: E-cadherin, vimentin, poly ADP-ribose polymerase (PARP), GAPDH (Cell Signaling Technology, Danvers, MA, USA) and ZEB1 (Santa Cruz Biotechnology, Dallas, TX, USA). The secondary antibody was HRP-conjugated anti-mouse or anti-rabbit IgG (Santa Cruz Biotechnology, Dallas, TX, USA). To detect specific signals, the membrane was examined using the ECL Prime Western Blotting Detection System (GE Healthcare, Amersham, UK) and LAS-3000 (Fujifilm, Tokyo, Japan). The relative band intensities were quantified using ImageJ software (National Institute of Health, Bethesda, MD, USA).

Results

Drug repositioning analysis for reversion of EMT signatures.

We previously reported the EMT status in 34 non-small cell lung cancer (NSCLC) cell lines (14). The EMT status was determined based on the protein expressions of E-cadherin, vimentin, N-cadherin, ZEB1, and ZEB2 evaluated using western

blotting analyses and the expressions of miR-200s, which are microRNAs known to be key players in the regulation of EMT features, evaluated using qPCR. For this study, we extracted 28 cell lines for which comprehensive gene expression data were available in the CCLE database (http://www.broadinstitute.org/ccle/), and we stratified them into two groups: 12 cell lines with an epithelial-like phenotype, and 16 cell lines with a mesenchymal-like phenotype (Figure 1A). We then performed GSEA to investigate the validity of this classification, and we confirmed that the Epithelial_Mesenchymal_Transition gene set was significantly enriched in the mesenchymal-like phenotype group (Figure 1B). Next, to identify reagents with the potential to reverse the EMT, we conducted C-MAP analysis. C-MAP is a widely used computational method for drug repositioning, containing a large transcriptomic compendium of drug-treated human cancer cells (13, 15). By testing user-provided gene lists (query list) against a large number of transcriptional profiles, potentially bioactive small molecules can be screened (13, 15). Based on the transcriptional profiles of 28 NSCLC cell lines, we selected 87 “epithelial-like” probes with positive correlations to mir-200c expression, including CDH1, as well as 52 “mesenchymal-like” probes with negative correlations to mir-200c expression, including ZEB1. We then used these probes as a query list for

comparisons with the rank-ordered lists for each drug treatment in the C-MAP database. We identified multiple Food and Drug Administration (FDA)-approved drugs with a significantly biased appearance of the query genes toward an epithelial-like feature (Table 1). The first ranked drug, thioridazine, is an antipsychotic drug; however, it was withdrawn from the market worldwide in 2005 because of its effect on the central nervous system and cardiotoxicity. We then focused on the second-ranked drug monensin, which is a polyether ionophore that is currently used as an antibiotic in livestock animals. The results of Kolmogorov-Smirnov scanning for monensin are shown in Figure 1C. Furthermore, all six independent experiments using different cell lines with different doses showed a positive effect on epithelial-like features (Figure 1D). In summary, this bioinformatics approach identified monensin as a candidate anti-EMT drug.

TGF-β stimulation facilitates EMT in cancer cells, leading to resistance to molecularly targeted therapy

TGF-β is a critical effector facilitating EMT through the modulation of Smad signaling, and TGF-β treatment is a well-established method for inducing the EMT *in vitro* (4). To assess the suppressive effect of monensin on the switch to EMT, we used TGF-β-induced EMT models *in vitro*. First, we examined the facilitating EMT effect of TGF-β in three NSCLC cell lines (A549, HCC827 and H1975) and one pancreatic cancer cell line (PANC-1). As expected, following TGF-β stimulation for 72 hours, these cells showed an up-regulation of the mesenchymal markers vimentin and ZEB1 and/or a down-regulation of the epithelial marker E-cadherin (Figure 2A). Morphological changes were also observed; some of the TGF-β-treated cells transformed to a spindle cell shape (Figure 2B), indicating that these cell lines acquired an EMT phenotype as a result of TGF-β treatment. Next, to determine the drug sensitivities of TGF-β-induced EMT cell models, we compared the sensitivity to osimertinib, an EGFR tyrosine kinase inhibitor, in the EGFR-mutant NSCLC cell lines HCC827 and H1975 in the presence or absence of TGF-β. In the absence of TGF-β, cell proliferation was effectively suppressed in both cell lines, whereas cells with TGF-β-induced EMT in the presence of TGF-β were less sensitive to osimertinib (Figure 2C). These results show that TGF-β stimulation induced EMT and that TGF-β-induced EMT NSCLC cell models are

useful for investigating EMT-mediated drug resistance.

Combined therapy with monensin as a therapeutic strategy for preventing EMT-mediated resistance

To validate the *in silico* findings of monensin as a candidate anti-EMT drug, we tested the inhibitory effect of monensin on the EMT using TGF-β-induced EMT cell models. Cells were cultured in the presence or absence of monensin and/or TGF-β for 72 hours, and the protein expressions of EMT markers were then analyzed. As shown in Figure 3A, the addition of monensin suppressed the up-regulation of vimentin by TGF-β stimulation in HCC827 and A549 cells; the up-regulation of ZEB1 in H1975, A549 and PANC-1 cells; and the down-regulation of E-cadherin in H827, H1975 and PAC-1 cells; although some of these changes were only slight. These results suggest that monensin has a partial inhibitory effect on TGF-β-induced EMT. We then examined the combinatorial effect on cell growth of osimertinib and monensin in cell viability assays to confirm whether acquired resistance to EGFR-TKI thorough TGF-β-induced EMT could be overcome by combination therapy with monensin. Treatment with monensin

alone showed some effect on cell growth, with IC_{50} values of 1.06 μM for HCC827 cells, 1.76 μM for H1975 cells, 0.74 μM for A549 cells, and 0.29 μM for PANC-1 cells (Figure 3B), and the addition of monensin restored the growth inhibitory effect of osimertinib in the two EGFR-mutant NSCLC cell lines with TGF-β-induced EMT (Figure 3C). To evaluate drug-induced apoptosis, cells were treated in the presence or absence of monensin and/or TGF-β for 72 hours, and the expression of the apoptosis marker cleaved-PARP was analyzed using western blotting. The expression of cleaved-PARP was suppressed by TGF-β treatment, while the addition of monensin restored the induction of apoptosis by osimertinib (Figure 3D). Taken together, these results showed that the addition of monensin could restore the growth inhibitory effect of osimertinib by preventing TGF-β-induced EMT.

Discussion

Acquired drug resistance against molecularly targeted therapy has been intensely studied especially in EGFR-mutant NSCLCs, and the most prominent

mechanism of the secondary EGFR T790M mutation can be targeted successfully using third-generation drugs such as osimertinib (16). However, the long-term clinical benefits remain unsatisfactory because a diversity of other mechanisms also contribute to drug resistance. One of the key mechanisms of resistance is the acquisition of an EMT signature, which is involved in not only molecularly targeted drugs, but also chemotherapy with cytotoxic drugs or radiation therapy in diverse cancer types (17-19). Therefore, a novel therapeutic strategy to overcome this resistance is a promising approach to improving outcomes. In the present study, we used a bioinformatics approach using C-MAP analysis to search for drugs with the potential to revert the EMT, and we identified monensin as a candidate anti-EMT drug. *In vitro* validation analyses demonstrated that monensin inhibited EMT conversion and improved drug response.

Monensin is a polyether ionophore antibiotic that is known to be a promoter of muscle growth in veterinary medicine. Monensin has been added to cattle and poultry feed for years and has a positive safety profile (11). Prior to this study, monensin had been reported to exhibit an anti-cancer effect by inhibiting cell proliferation, cell cycle progression and cell migration and by inducing cell

apoptosis in diverse cancer types, such as lung cancer, pancreatic cancer, renal cancer, colon cancer, prostate cancer, and ovarian cancer (20-24). Of note, malignant cells were 20-fold more sensitive to monensin than normal cells, indicating that monensin could be a cancer-specific therapeutic drug (22). Mechanically, monensin has been shown to induce a Golgi apparatus stress response, mitochondrial damage, and oxidative stress, initiating signaling pathways to trigger apoptosis through the up-regulation of Bax, caspase-3 and caspase-8 (22, 24, 25). Monensin has also been reported to target multiple signaling pathways, such as EGFR, Hedgehog, Wnt, CDK6, cyclin D1, and cyclin A, as well as multiple transcript factors, including E2F/DP1, STAT1/2, NFκB, AP-1 and Elk-1/SRF (20, 21, 23, 24, 26). Of note, Vanneste et al. conducted a systematic high throughput screening for compounds with anti-EMT activity and demonstrated that EMT-like cells exhibited a greater uptake of monensin compared with cells with epithelial features, leading to a selective cytotoxic effect on an EMT phenotype (25). However, our data using an isogenic NSCLC cell line model showed no relationships between the sensitivity to monensin and the EMT status (Supplementary Figure 1A and 1B). Specifically, we established a distinct isogenic cell model using HCC827 cells that had been chronically exposed to

osimertinib, and the resistant cells acquired an EMT phenotype (Supplementary Figure 1A), leading to EMT-mediated drug resistance to EGFR-TKI and cytotoxic reagents (27). In terms of sensitivity to monensin, unexpectedly, no significant differences were observed between the parental cells and the resistant cells despite their different EMT statuses (Supplementary Figure 1B). Furthermore, monensin treatment did not restore the epithelial phenotype (Supplementary Figure 2A) or the sensitivity to EGFR-TKI in the resistant cells with EMT conversion (Supplementary Figure 2B). Considering these findings, monensin might not have a direct effect on the EMT signatures in our resistant cells, and the inhibition of EMT conversion might be obtained through the suppression of some EMT-facilitating factors, including TGF-β. Furthermore, its effect likely differs depending on the cancer type. Further study is warranted to elucidate this intriguing biological mechanism.

In the 1990s, the calcium channel blocker verapamil was tested in a clinical trial as a chemosensitizer to reverse drug resistance by inhibiting a drug efflux pump, which is the one of the key functions of EMT-mediated resistance. However, because of the dose-limiting toxicity, verapamil did not show any clear evidence of a beneficial effect on cytotoxic chemotherapy reagents (1). Monensin has been

approved by the FDA for veterinary use and has been shown to have a positive biosafety profile in veterinary medicine. In previous studies, the antitumor activity of monensin was demonstrated in an *in vivo* model, and no significant adverse effects were seen even at a much higher dose of monensin than the 100-nM dose used in the present study(20, 23). Nonetheless, in attempting to translate our findings clinically, careful assessment of any possible toxic effects of long-term use in humans is warranted prior to repositioning monensin as a combinatory therapy with standard antitumor reagents.

In conclusion, the current study demonstrated the possible utility of monensin as a prophylactic when co-administered with antitumor reagents to prevent the acquisition of an EMT signature, thereby prolonging the disease-control period.

Tables and Figures

A

EMT status	Names of cell lines	Number of cell lines
Epithelial-like type	CALU3, NCI-H1975, NCI-H441, HCC827, NCI-H2170, NCI-H1781, HCC4006, NCI-H3255, NCI-H1666, NCI-H1648, PC14, HCC2935	12
Mesenchymal-like type	NCI-H1299, NCI-H522, NCI-H23, NCI-H2087, A549, NCI-H2009, NCI-H661, NCI-H838, HCC2279, NCI-H460, HCC366, HCC364, NCI-H1650, NCI-H358, NCI-H1395, NCI-H2228	16

B

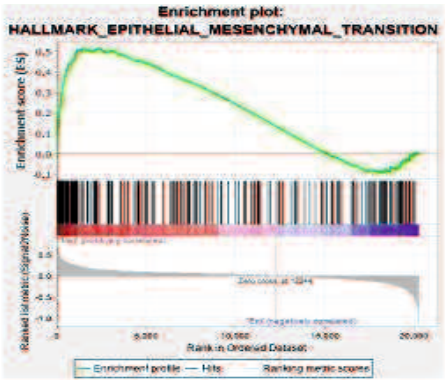

C

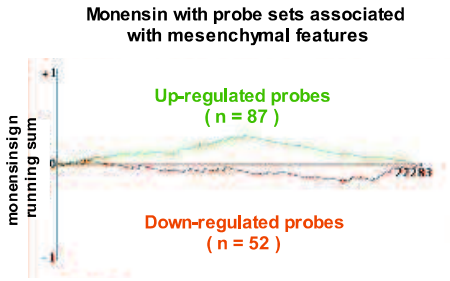

D

rank	cmap name	dose	cell line	score
21	monensin	6 μM	MCF7	0.762
34	monensin	6 μM	PC3	0.721
94	monensin	6 μM	MCF7	0.658
506	monensin	11 μM	MCF7	0.509
631	monensin	6 μM	PC3	0.483
2859	monensin	6 μM	HL60	0

Figure 1. Identification of reagents with the potential to reverse the EMT using C-MAP analysis. A, Classification of 28 NSCLC cell lines according to their EMT status. B, Representative GSEA enrichment plots for the Epithelial Mesenchymal Transition gene sets for 28 NSCLC cell lines. C, Representative results of Kolmogorov-Smirnov scanning showing an enrichment of outcome-associated probe sets for the 4th ranked monensin, indicating the up-regulation of 87 epithelial-like probes and the down-regulation of 52 mesenchymal-like probes. D,

Summaries of all instances of monensin. The barview shows the instances of monensin in a total of 6100 instances.

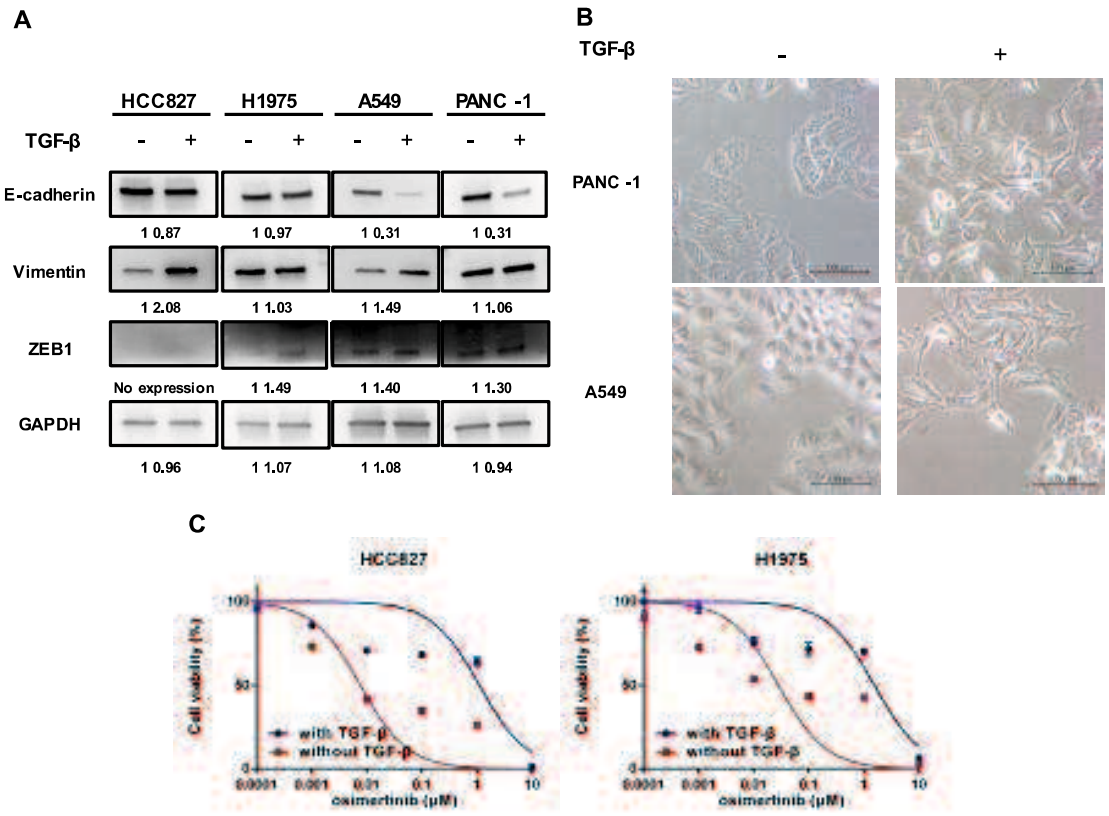

Figure 2. Establishment of TGF-β-induced EMT models using three NSCLC cell lines and one pancreatic cancer cell line. A, Cells were treated with TGF-β (2 ng/mL) for 72 hours and then subjected to immunoblotting. The relative band intensity was quantified using a densitometric analysis with ImageJ software. B, PANC-1 and A549 cells were treated with TGF-β (2 ng/mL) for 5 days; representative microscopy images are shown. The scale bar represents 100 nm. C, HCC827 and H1975 cells were pretreated with TGF-β (2 ng/mL) for 24 hours and were then subsequently treated with osimertinib for 96 hours. Cell viability was determined using CellTiter 96 Aqueous bromide dye. Each experiment was

assayed in eight replicate determinations, and the data are representative of three independent experiments (mean ± SE).

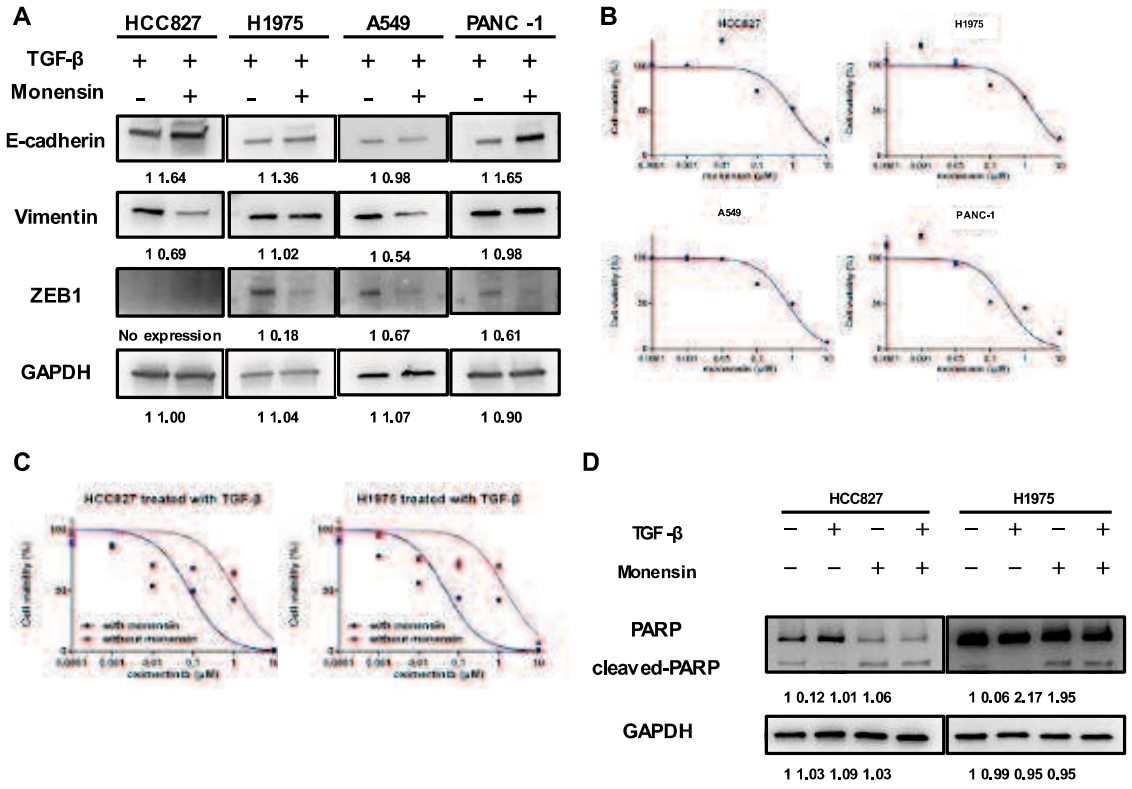

Figure 3. Monensin restores the growth inhibitory effect of osimertinib through the prevention of TGF-β-induced EMT. A, Cells were cultured in the presence or absence of monensin (100 nM) and/or TGF-β (2 ng/mL) for 72 hours, then subjected to immunoblotting. The relative band intensity was quantified using a densitometric analysis with ImageJ software. B, Cells were treated with monensin for 96 hours. Cell viability was determined using CellTiter 96 aqueous bromide dye. Each experiment was assayed in eight replicate determinations, and the data are representative of three independent experiments (mean ± SE). C, HCC827 and H1975 cells were pretreated with TGF-β (2 ng/mL) in the presence

or absence of monensin (100 nM) for 24 hours, then subsequently treated with osimertinib for 96 hours. Cell viability was determined using CellTiter 96 Aqueous bromide dye. Each experiment was assayed in eight replicate determinations, and data are representative of three independent experiments (mean ± SE). D, HCC827 and H1975 cells were pretreated with TGF-β (2 ng/mL) in the presence or absence of monensin (100 nM) for 24 hours, then followed by osimertinib treatment for 72 hours.

Rank	cmap name	n	Enrichment	P value
1	thioridazine	182	0.475	0.0001
2	monensin	20	0.731	0.00101
3	sulfamonomethoxine	12	0.806	0.00265
4	mebeverine	6	0.801	0.00298
5	perphenazine	4	0.726	0.00348
6	zuclopenthixol	4	0.782	0.0042
7	oxamniquine	4	0.782	0.00422
8	gibberellic acid	5	0.764	0.00585
9	phentolamine	4	0.599	0.00605
10	meclofenamic acid	4	0.695	0.00655

Table 1 Permuted results of C-MAP analysis (top 20 list of reagent)

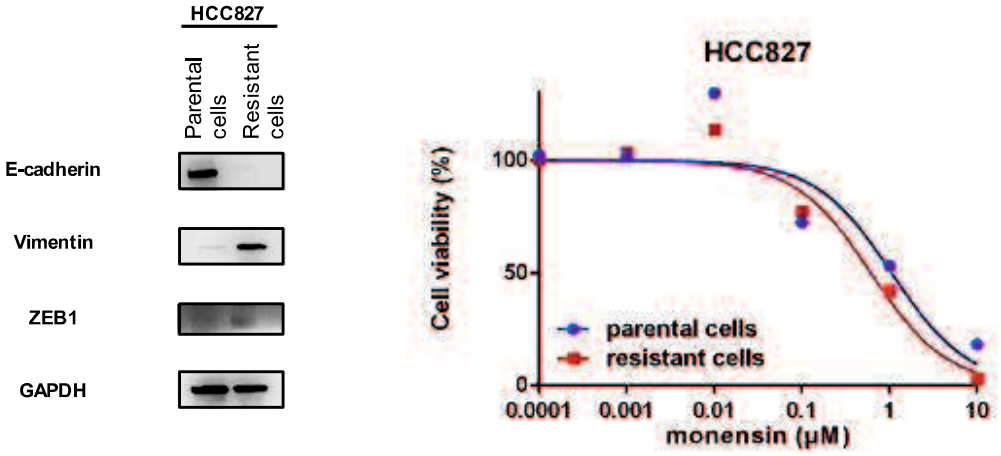

Fig. S1 Assessment of the relationships between the sensitivity to monensin and EMT features. A, Osimertinib resistant batch was established by the chronic exposure, showing acquired EMT phenotype. B, HCC827 parental cells and osimertinib resistant cells were treated with monensin for 96 hours. Cell viability was determined using CellTiter 96 Aqueous bromide dye.

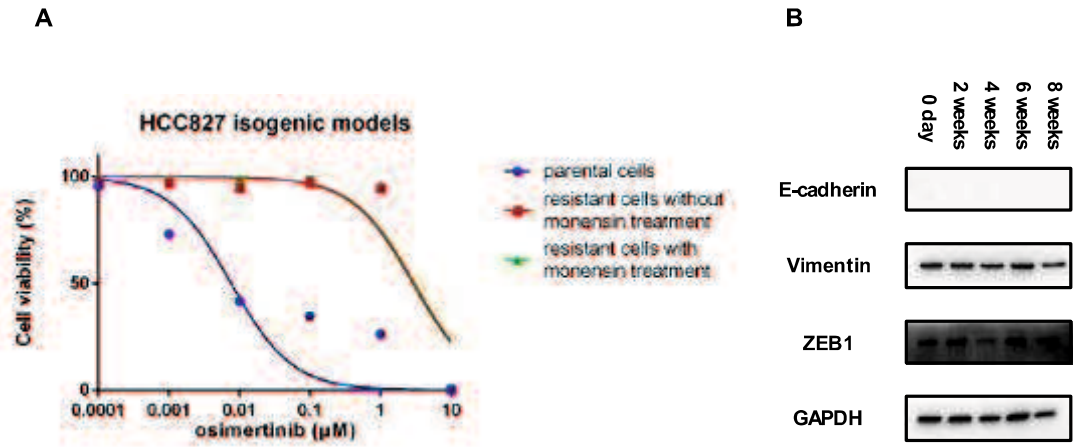

Fig. S2 Monensin treatment didn't restore epithelial phenotype and sensitivity to EGFR-TKI in the resistant cells with EMT conversion

A, HCC827 parental cells, resistant cells without monensin treatment cells and resistant cells with monensin treatment for 8 weeks were treated with osimertinib for 96 hours. Cell viability was determined using CellTiter 96 Aqueous bromide dye. B, HCC827 Osimertinib resistant cells acquiring EMT features were treated with monensin for indicated time, and then subjected to immunoblotting.

References

1. B. Du, J.S. Shim, Targeting Epithelial-Mesenchymal Transition (EMT) to Overcome Drug Resistance in Cancer, Molecules (Basel, Switzerland), 21 (2016).
2. A. Singh, J. Settleman, EMT, cancer stem cells and drug resistance: an emerging axis of evil in the war on cancer, Oncogene, 29 (2010) 4741-4751.
3. K. Horiguchi, K. Sakamoto, D. Koinuma, K. Semba, A. Inoue, S. Inoue, H. Fujii, A. Yamaguchi, K. Miyazawa, K. Miyazono, M. Saitoh, TGF-beta drives epithelial-mesenchymal transition through deltaEF1-mediated downregulation of ESRP, Oncogene, 31 (2012) 3190-3201.
4. J. Xu, S. Lamouille, R. Derynck, TGF-beta-induced epithelial to mesenchymal transition, Cell Res., 19 (2009) 156-172.
5. K.R. Fischer, A. Durrans, S. Lee, J. Sheng, F. LihS.T. Wong, H. ChoihT. El Rayes, S. RyuhJ. Troeger, R.F. Schwabe, L.T. Vahdat, N.K. Altorki, V. Mittal, D. Gao, Epithelial-to-mesenchymal transition is not required for lung metastasis but contributes to chemoresistance, Nature, 527 (2015) 472-476.
6. K. Shien, S. Toyooka, H. Yamamoto, J. Soh, M. Jida, K.L. Thu, S. Hashida, Y. Maki, E. Ichihara, H. Asano, K. Tsukuda, N. Takigawa, K. Kiura, A.F. Gazdar, W.L. Lam, S. Miyoshi, Acquired resistance to EGFR inhibitors is associated with a manifestation of stem cell-like properties in cancer cells, Cancer Res, 73 (2013) 3051-3061.
7. S. Hashida, H. Yamamoto, K. Shien, Y. Miyoshi, T. Ohtsuka, K. Suzawa, M. Watanabe, Y. Maki, J. Soh, H. Asano, K. Tsukuda, S. Miyoshi, S. Toyooka, Acquisition of cancer stem cell-like properties in non-small cell lung cancer with acquired resistance to afatinib, Cancer Sci, 106 (2015) 1377-1384.
8. M. Saitoh, Epithelial-mesenchymal transition is regulated at post-transcriptional levels by transforming growth factor-beta signaling during tumor progression, Cancer Sci., 106 (2015) 481-488.
9. T.T. Ashburn, K.B. Thor, Drug repositioning: identifying and developing new uses for existing drugs, Nature reviews. Drug discovery, 3 (2004) 673-683.
10. T.J. Yang, T.S. Yang, H.M. Liang, Thalidomide and congenital abnormalities, Lancet, 1 (1963) 552-553.
11. B.C. Pressman, Biological applications of ionophores, Annu. Rev. Biochem., 45 (1976) 501-530.
12. A. Subramanian, P. Tamayo, V.K. Mootha, S. Mukherjee, B.L. Ebert, M.A. Gillette, A. Paulovich, S.L. Pomeroy, T.R. Golub, E.S. Lander, J.P. Mesirov, Gene set enrichment analysis: a knowledge-based approach for interpreting genome-wide expression profiles, Proc. Natl. Acad. Sci. U. S. A., 102 (2005) 15545-15550.

13. J. Lamb, E.D. Crawford, D. Peck, J.W. Modell, I.C. Blat, M.J. Wrobel, J. Lerner, J.P. Brunet, A. Subramanian, K.N. Ross, M. Reich, H. Hieronymus, G. Wei, S.A. Armstrong, S.J. Haggarty, P.A. Clemons, R. Wei, S.A. Carr, E.S. Lander, T.R. Golub, The Connectivity Map: using gene-expression signatures to connect small molecules, genes, and disease, Science, 313 (2006) 1929-1935.
14. H. Sato, K. Shien, S. Tomida, K. Okayasu, K. Suzawa, S. Hashida, H. Torigoe, M. Watanabe, H. Yamamoto, J. Soh, H. Asano, K. Tsukuda, S. Miyoshi, S. Toyooka, Targeting the miR-200c/LIN28B axis in acquired EGFR-TKI resistance non-small cell lung cancer cells harboring EMT features, Sci. Rep., 7 (2017) 40847.
15. H. Ebi, S. Tomida, T. Takeuchi, C. Arima, T. Sato, T. Mitsudomi, Y. Yatabe, H. Osada, T. Takahashi, Relationship of deregulated signaling converging onto mTOR with prognosis and classification of lung adenocarcinoma shown by two independent in silico analyses, Cancer Res, 69 (2009) 4027-4035.
16. T.S. Mok, Y.L. Wu, M.J. Ahn, M.C. Garassino, H.R. Kim, S.S. Ramalingam, F.A. Shepherd, Y. He, H. Akamatsu, W.S. Theelen, C.K. Lee, M. Sebastian, A. Templeton, H. Mann, M. Marotti, S. Ghiorghiu, V.A. Papadimitrakopoulou, Osimertinib or Platinum-Pemetrexed in EGFR T790M-Positive Lung Cancer, N. Engl. J. Med., 376 (2017) 629-640.
17. A.D. Yang, F. Fan, E.R. Camp, G. van Buren, W. Liu, R. Somcio, M.J. Gray, H. Cheng, P.M. Hoff, L.M. Ellis, Chronic oxaliplatin resistance induces epithelial-to-mesenchymal transition in colorectal cancer cell lines, Clin Cancer Res, 12 (2006) 4147-4153.
18. J.H. Chung, J.K. Rho, X. Xu, J.S. Lee, H.I. Yoon, C.T. Lee, Y.J. Choi, H.R. Kim, C.H. Kim, J.C. Lee, Clinical and molecular evidences of epithelial to mesenchymal transition in acquired resistance to EGFR-TKIs, Lung Cancer, 73 (2011) 176-182.
19. L. Chang, P.H. Graham, J. Hao, J. Bucci, P.J. Cozzi, J.H. Kearsley, Y. Li, Emerging roles of radioresistance in prostate cancer metastasis and radiation therapy, Cancer Metastasis Rev, 33 (2014) 469-496.
20. X. Wang, X. Wu, Z. Zhang, C. Ma, T. Wu, S. Tang, Z. Zeng, S. Huang, C. Gong, C. Yuan, L. Zhang, Y. Feng, B. Huang, W. Liu, B. Zhang, Y. Shen, W. Luo, X. Wang, B. Liu, Y. Lei, Z. Ye, L. Zhao, D. Cao, L. Yang, X. Chen, R.C. Haydon, H.H. Luu, B. Peng, X. Liu, T.C. He, Monensin inhibits cell proliferation and tumor growth of chemo-resistant pancreatic cancer cells by targeting the EGFR signaling pathway, Sci. Rep., 8 (2018) 17914.
21. K. Dayekh, S. Johnson-Obaseki, M. Corsten, P.J. Villeneuve, H.S. Sekhon, J.I. Weberpals, J. Dimitroulakos, Monensin inhibits epidermal growth factor receptor trafficking and activation: synergistic cytotoxicity in combination with EGFR inhibitors, Mol Cancer Ther, 13 (2014) 2559-2571.
22. K. Ketola, P. Vainio, V. Fey, O. Kallioniemi, K. Iljin, Monensin is a potent inducer of oxidative

stress and inhibitor of androgen signaling leading to apoptosis in prostate cancer cells, Mol Cancer Ther, 9 (2010) 3175-3185.

23. Y. Deng, J. Zhang, Z. Wang, Z. Yan, M. Qiao, J. Ye, Q. Wei, J. Wang, X. Wang, L. Zhao, S. Lu, S. Tang, M.K. Mohammed, H. Liu, J. Fan, F. Zhang, Y. Zou, J. Liao, H. Qi, R.C. Haydon, H.H. Luu, T.C. He, L. Tang, Antibiotic monensin synergizes with EGFR inhibitors and oxaliplatin to suppress the proliferation of human ovarian cancer cells, Sci. Rep., 5 (2015) 17523.
24. W.H. Park, M.S. Lee, K. Park, E.S. Kim, B.K. Kim, Y.Y. Lee, Monensin-mediated growth inhibition in acute myelogenous leukemia cells via cell cycle arrest and apoptosis, Int J Cancer, 101 (2002) 235-242.
25. M. Vanneste, Q. Huang, M. Li, D. Moose, L. Zhao, M.A. Stamnes, M. Schultz, M. Wu, M.D. Henry, High content screening identifies monensin as an EMT-selective cytotoxic compound, Sci. Rep., 9 (2019) 1200.
26. J. Mao, S. Fan, W. Ma, P. Fan, B. Wang, J. Zhang, H. Wang, B. Tang, Q. Zhang, X. Yu, L. Wang, B. Song, L. Li, Roles of Wnt/beta-catenin signaling in the gastric cancer stem cells proliferation and salinomycin treatment, Cell Death Dis., 5 (2014) e1039.
27. K. Namba, K. Shien, Y. Takahashi, H. Torigoe, H. Sato, T. Yoshioka, T. Takeda, E. Kurihara, Y. Ogoshi, H. Yamamoto, J. Soh, S. Tomida, S. Toyooka, Activation of AXL as a Preclinical Acquired Resistance Mechanism Against Osimertinib Treatment in EGFR-Mutant Non-Small Cell Lung Cancer Cells, Mol Cancer Res, 17 (2019) 499-507.

CHAPTER 2

Drug repositioning of tranilast to sensitize a cancer therapy by targeting cancer-associated fibroblast

Abstract

Cancer-associated fibroblasts (CAFs) are a major component of the tumor microenvironment that mediate resistance of cancer cells to anticancer drugs. Tranilast is an antiallergic drug that suppresses the release of cytokines from various inflammatory cells. In this study, we investigated the inhibitory effect of tranilast on the interactions between non-small cell lung cancer (NSCLC) cells and the CAFs in the tumor microenvironment. Three *EGFR*-mutant NSCLC cell lines, two *KRAS*-mutant cell lines and three CAFs derived from NSCLC patients were used. To mimic the tumor microenvironment, the NSCLC cells were co-cultured with the CAFs *in vitro*, and the molecular profiles and sensitivity to molecular targeted therapy were assessed. Crosstalk between NSCLC cells and CAFs induced multiple biological effects on the NSCLC cells both *in vivo* and *in vitro*, including activation of the STAT3 signaling pathway, promotion of xenograft tumor growth, induction of epithelial-mesenchymal transition (EMT), and

acquisition of resistance to molecular-targeted therapy, including of *EGFR*-mutant NSCLC cells to osimertinib and of *KRAS*-mutant NSCLC cells to selumetinib. Treatment with tranilast led to inhibition of IL-6 secretion from the CAFs, which, in turn, resulted in inhibition of CAF-induced phospho-STAT3 upregulation. Tranilast also inhibited CAF-induced EMT in the NSCLC cells. Finally, combined administration of tranilast with molecular-targeted therapy reversed the CAF-mediated resistance of the NSCLC cells to the molecular-targeted drugs, both *in vitro* and *in vivo*. Our results showed that combined administration of tranilast with molecular-targeted therapy is a possible new treatment strategy to overcome drug resistance caused by cancer- CAF interaction.

Introduction

Lung cancer is the leading cause of cancer death worldwide (1). Significant advances have been made in the treatment of non-small cell lung cancer (NSCLC) with the development of drugs targeting oncogenic driver mutations or immune checkpoint molecules (2), which have enabled precision

medicine. However, while most molecular-targeted therapies initially show significant effect, acquired resistance to the drugs eventually develops; and efforts are being made to develop complementary therapies to maximize the effects of the targeted therapies or overcome the acquired drug resistance. A variety of resistance mechanisms to anticancer drugs, especially to molecular-targeted drugs, have been elucidated, including second-site mutations in the kinase domain, bypass signaling pathway activation, copy number changes, and histologic transformation (3,4), although many questions still remain.

Cancer-related fibroblasts (CAFs) are one of the major components of the tumor stroma and contribute significantly to the tumor microenvironment. It has been shown that CAFs release several cytokines, such as interleukin-6 (IL-6), TGF-β and epidermal growth factor (EGF), which activate multiple signaling pathways in cancer cells to promote tumor cell proliferation, invasion, metastasis and chemoresistance (5-8). It has been reported that activation of the IL-6/STAT3 signaling pathway in NSCLC cells by substances secreted by CAFs is a critical contributor to CAF-mediated drug resistance (5).Therefore, CAF-targeted therapy is gaining attention as one of the complementary treatment strategies for cancer.

Drug repositioning (or repurposing/reprofiling) is the process of finding new therapeutic indications for existing drugs. It is an attractive approach toward rapid drug discovery and development at a relatively low-cost and high efficiency, because clinical and pharmacokinetic data of existing drugs are already established (9). One of the most notable examples of a repositioned drug is thalidomide, which was initially developed for morning sickness and was subsequently successfully repositioned as an anticancer drug for multiple myeloma (9).

Here, we examined the usefulness of tranilast (N-[3,4-dimethoxycinnamoyl]-anthranilic acid) as a possible therapeutic agent for targeting CAFs. Tranilast is an anti-allergic drug that is used clinically for bronchial asthma and hypertrophic scars (10). The drug is known to suppress collagen production and release of TGF-β from fibroblasts (11) and of IL-11 from macrophages (12). In this study, we investigated the microenvironmental interactions between the CAFs and NSCLC cells in co-culture models *in vitro and in vivo*. We then assessed the inhibitory effect of tranilast on their crosstalk and its potential to overcome CAF-mediated acquisition of drug resistance in cancer treatment.

Materials and methods

Cell culture and reagents

Three *EGFR*-mutant NSCLC cell lines (HCC827 [EGFR exon19del E746-A750], HCC4011 [EGFR L858R], and PC9 [EGFR exon19del E746-A750]) and two *KRAS*-mutant NSCLC cell lines (H23 [KRAS G12C] H2009 [KRAS G12A]) were used in this study. All the NSCLC cell lines were purchased from the American Type Culture Collection (Manassas, VA, USA). Three CAFs named CAF1, CAF2, and CAF3 were obtained from surgically resected 3 NSCLC specimens derived from each 3 patient, immortalized by retroviral transduction of *hTERT* to stabilize the cell phenotype and avoid cellular senescence, and cultured in Roswell Park Memorial Institute (RPMI)-1640 medium supplemented with 10% fetal bovine serum at 37 ºC in a humidified incubator under 5% CO_2. Studies using clinical specimens were approved by the Okayama Medical School and Hospital's Research Ethics Committee (Approval Number: # 1906-033), and informed consent was obtained from individual patients for the use of their materials. Osimertinib, an EGFR-tyrosine kinase inhibitor, was purchased from ChemScene (Monmouth Junction, NJ, USA), selumetinib, an MEK inhibitor, was purchased from Selleckchem (Houston, TX, USA). and tranilast was purchased from Tokyo

Chemical Industry (Tokyo, Japan).

Co-culture of NSCLC cells with fibroblasts

Cancer cells were placed in the bottom compartment (2×10^4 cells per chamber) and CAFs (2×10^5) in the top compartment of transwell polycarbonate membrane cell culture inserts placed in a 6-well plate; the bottom and top compartments were separated by a filter with a pore size of 0.4 mm (SARSTEDT, Germany).

Cell viability assay

The sensitivity to each drug was determined by the MTS assay. Cells were plated at a density of 3,000 cells per well in 96-well plates, and treated with a preset concentration of each drug. Cell viability was assayed after 72 hours of treatment using the CellTiter 96 Aqueous bromide One Solution Reagent (Promega, Madison, WI, USA). For measurement of the IC_{50} value, eight-replicate determinations were obtained in three independent experiments. Data were analyzed by non-linear regression, using Graphpad Prism Ver. 6.0.3 (GraphPad Software, San Diego, CA).

Western blotting

The total cell lysate was extracted with a lysis buffer, a mixture of RIPA buffer, phosphate inhibitor cocktails 2 and 3 (Sigma-Aldrich, St. Louis, MO, USA) and complete Mini Protease Inhibitor Cocktail (Roche, Switzerland). Western blot analysis was performed using the following primary antibodies: STAT3, p-STAT3 (Tyr705), E-cadherin, vimentin, IL-6 (D3K2N), and GAPDH (Cell Signaling Technology, Danvers, MA, USA). The secondary antibody used was HRP-conjugated anti-rabbit IgG (Santa Cruz Biotechnology, Dallas, TX, USA). We evaluated the substances secreted from the CAFs into the culture medium by the centrifugal filter device Amicon Ultra 10K (Pall, Port Washington, NY, USA). To detect specific signals, the membrane was examined using the ECL Prime Western Blotting Detection System (GE Healthcare, Amersham, UK) and LAS-3000 (Fujifilm, Tokyo, Japan). The relative band intensities were quantified using ImageJ software (National Institute of Health, Bethesda, MD, USA).

Gene expression assay

Total RNA from cultured cells was isolated using the RNeasy Mini Kit (Qiagen) and reverse-transcribed with the High Capacity cDNA Reverse Transcription Kit

(Thermo Fisher Scientific). Quantitative RT-PCR (qRT-PCR) was performed on the StepOnePlus Real-Time PCR System (Thermo Fisher Scientific) using TaqMan Gene Expression Assays (Thermo Fisher Scientific). The gene expression levels were calculated using the delta-delta CT method. GAPDH was used as the endogenous control. The assays were repeated three times. Data are expressed as the means ± SE.

Colony formation assay

Cancer cells (2×10^4 cells per chamber) were cultured in a 6-well plate with or without CAFs (2×10^5) placed in the top compartment of a transwell polycarbonate membrane cell culture insert, and treated with the molecular-targeted drugs and tranilast for 7 days. After fixation in 4% formaldehyde, the cells were stained using 0.2% crystal violet. Colony counts were measured using the ImageJ software (National Institutes of Health, Bethesda, MD).

Xenograft mouse model

Four-week-old BALB/c-nu/nu female mice were purchased from Charles River Laboratories (Yokohama, Japan). All mice were provided with sterilized food and

water and housed in a barrier facility under a 12:12-hour light-dark cycle. PC9 cells (1×10^6), CAF1 cells (1×10^6), or PC9 cells (5×10^5) mixed with CAF1 cells (5×10^5) (1:1 ratio) were suspended in 100 μL of RPMI-1640 with Matrigel Basement Membrane Matrix (Corning) mixture (1:1 ratio) and injected subcutaneously into the backs of the mice. The tumor xenografts were measured using digital calipers, and the tumor volumes were calculated using the formula, volume=1/2×([shortest diameter]^2×[longest diameter]). When the tumor volumes exceeded approximately 150 mm^3, the mice were randomly allocated to one of four groups: the control group, the osimertinib (5 mg/kg/d) group, the tranilast (200 mg/kg/d) group, and the osimertinib (5 mg/kg/d) plus tranilast (200 mg/kg/d) group (n=7 per group). The drugs were suspended in 0.5 w/v (%) methylcellulose and administered by oral gavage five times a week. The tumor volumes were measured twice a week. For analysis of apoptosis, formalin fixed and paraffin embedded (FFPE) tissue samples from the xenograft tumors were stained using the DeadEnd Fluorometric TUNEL System (PROMEGA, Madison, WI, USA). The cells were counter-stained with 4',6-diamidino-2-phenylindole (DAPI). The number of positively stained cells as a percentage of the total number of cells was counted under a fluorescence microscope in five random fields and averaged.

Data are expressed as the mean ± SE. The protocol for the animal experiments was approved by the Animal Care and Use Committee, Okayama University (Permit Number: OKU-2020564).

Results

CAFs facilitate the malignant behaviors of NSCLC cells

To assess the microenvironmental interactions between the CAFs and NSCLC cells, we performed co-culture of NSCLC cell lines with CAFs using the Boyden-chamber system, and evaluated the changes in the phosphorylation status of STAT3 in the NSCLC cells by Western blotting. As expected, co-culture of NSCLC cells with CAFs increased phospho-STAT3 in PC9 cells (Fig. 1A). Next, the role of CAFs within a tumor on the tumor growth was evaluated *in vivo*. PC9 cells alone or PC9 cells plus CAF1 cells were subcutaneously implanted into the flanks of nude mice. As shown in Figure 1B, the group that received subcutaneous implantation of PC9 cells plus CAFs showed more aggressive growth of the tumors; no mass formation was observed in the group that received subcutaneous implantation of CAFs alone. Next, we examined the effect of CAFs

in facilitating EMT in the tumor cells. As shown in Figure 1C, HCC4011 cells cultured with CAFs showed morphological changes to a spindle shape and elongated formation as compared to control cells cultured without CAFs, while the differences were not clear in other cell lines (Supplementary Fig. S1A). Furthermore, HCC4011, H2009 and H23 cells showed upregulation of the mesenchymal marker vimentin, but on the other hand, PC9 and HCC827 cells didn't show significant changes (Fig. 1D and Supplementary Fig. S1B). It suggests that CAF induces EMT in the NSCLC cells, while the tendency to undergo EMT differs depending on the cell line. We also investigated the acquisition of drug resistance mediated by CAFs in the *in vivo* model. Mice bearing tumor xenografts of PC9 cells alone or of PC9 cells plus CAF1 cells were treated with osimertinib (5 mg/kg) by oral gavage five times a week. Osimertinib treatment was less effective at slowing the growth of tumor xenografts of PC9 cells plus CAFs than of tumor xenografts of PC9 cells alone (Fig. 1E).

Tranilast suppresses STAT3 activation via decrease of CAF-derived IL-6 and inhibits EMT

We examined the inhibitory effect of tranilast on CAF-induced-STAT3 activation

and EMT in the NSCLC cells. Treatment with tranilast alone showed little effect on the cell growth of any of the 5 lung cancer cell lines or 3 CAFs, with IC_{50} values of 150-250 μM (Supplementary Fig. S2). Next, cancer cells were cultured with or without CAF1 cells for one week in the presence or absence of 100 μM tranilast, and the protein expressions of STAT3 and EMT markers in the tumor cells were analyzed. Co-culture with CAFs increased the expression level of pSTAT3 in the tumor cells, and tranilast inhibited CAF-mediated pSTAT3 activation (Fig. 2A). Identical results were confirmed using the other sublines of CAFs (Supplementary Fig. S3). To further explore the mechanism of STAT3 suppression by tranilast, we examined the expression of IL-6, a cytokine that activates the JAK1/STAT3 signaling pathway. Treatment with tranilast for 48 hours decreased the mRNA expression of IL6 in CAFs (Fig. 2B) and of IL-6 secretion from CAFs into the culture medium (Fig. 2C). In terms of the inhibitory effect on EMT, tranilast decreased the expression of vimentin in the tumor cells, suggesting a partial inhibitory effect on CAF-induced EMT (Fig. 2D). This finding was also confirmed with the other CAF sublines (Supplementary Fig S4). Next, HCC4011 and H2009 cells were treated with IL-6 (1 ng/mL) for 72 hours, and the EMT status was analyzed by Western blotting to assess whether the EMT

inhibitory effect by tranilast was due to the suppressive effect on IL-6 secretion from CAFs. However, IL-6 treatment did not induce EMT in this model (data not shown). Furthermore, a TGF-β-induced EMT model was used to evaluate the direct effect of tranilast on the cancer cells. As shown in Figure 2E and 2F, following TGF-β (3 ng/mL) stimulation, HCC4011 cells showed morphological changes to a spindle shape and elongated formation, and HCC4011 and H2009 cells showed upregulation of vimentin, suggesting the occurrence of EMT in the cells; however, addition of tranilast showed a partial inhibitory effect on TGF-β-induced EMT (Fig. 2G). These results suggest that tranilast directly prevents EMT of cancer cells, although the detailed mechanisms still remain elusive.

Combined treatment with tranilast plus molecular-targeted drugs suppressed the growth of NSCLC cells in an *in vitro* co-culture model of NSCLC cells and CAFs

In the section above, we described the inhibitory effects of tranilast on STAT3 activation and EMT in cancer cells, which suggests that combined administration of tranilast with molecular-targeted agents may be an effective therapeutic strategy to counter CAF-mediated acquisition of drug resistance. Therefore, we

assessed the efficacy of combined tranilast plus osimertinib or selumetinib treatment in an *in vitro* co-culture model of NCSLC cells and CAFs. Tranilast treatment alone showed a minimal inhibitory effect on the growth of the cancer cells, while osimertinib/selumetinib treatment alone showed a strong growth-inhibitory effect in the *EGFR*-mutant/*KRAS*-mutant lung cancer cells. When the cancer cells were co-cultured with CAFs, they were less sensitive to the aforementioned treatments; however, combined tranilast plus osimertinib/selumetinib treatment resulted in improved cancer cell sensitivity to osimertinib/selumetinib (Fig. 3A). Similar results were obtained with the other CAF sublines (Supplementary Fig. S5A and S5B). Quantification of the results using the ImageJ software revealed significant differences (Fig. 3B).

Combined tranilast plus osimertinib treatment inhibited tumor growth in a mouse xenograft model of *EGFR*-mutant NSCLC cells plus CAFs

To validate the aforementioned *in vitro* findings, we tested the efficacy of combined osimertinib plus tranilast treatment in a mouse mixed-cell (PC9 cells plus CAF1 cells) xenograft model. Mice bearing mixed-cell xenografts were treated with osimertinib alone, tranilast alone, or a combination of the two drugs.

Although tranilast alone was found to exert a mild inhibitory effect in the colony formation assay *in vitro*, tranilast monotherapy had minimal effect on the tumor growth *in vivo*. Osimertinib monotherapy caused only partial shrinkage of the tumor, whereas combined osimertinib plus tranilast treatment yielded an enhanced antitumor effect. The drug combination was well-tolerated throughout the 38-day treatment period (Fig. 4A). TUNEL staining showed the greatest number of apoptotic cells in the combined treatment group (Fig. 4B and C).

Discussion

Accumulating evidence indicates that the crosstalk between cancer cells and the tumor microenvironment (TME) plays critical roles in the processes involved in tumor progression, including cancer initiation, proliferation, invasion, and metastasis (13). CAFs are the major cellular components of the tumor microenvironment, that contribute significantly to tumor aggressiveness and drug resistance by producing various types of cytokines, chemokines, growth factors, and matrix-degrading enzymes (14). Therefore, disruption of the TME, especially targeting the CAFs, is attracting attention as a novel and critical complemental

therapeutic strategy to molecular-targeted treatment. In this study, we clarified the inhibitory effects of tranilast on CAF-induced enhancement of an aggressive tumor phenotype.

In addition to its use as an anti-allergic drug, tranilast is also widely used for the treatment to hypertrophic scars, and its safety for clinical use has already been demonstrated. Tranilast inhibits the release of biologically active mediators from mast cells, as well as VEGF-induced angiogenesis (10,15-17). In addition, tranilast has been reported to have direct anti-cancer effects by suppressing cancer cell proliferation, migration and invasion, and inhibiting tumor angiogenesis in diverse cancer types, such as breast cancer, gastric cancer, and esophageal cancer. Previous reports indicated that tranilast is generally used in high concentrations. (18-22). The major mechanism underlying the efficacy of tranilast is thought to be suppression of the cellular TGF-β signaling pathway by the drug, although other drug actions could have roles as well (23). On the basis of these preclinical findings, a phase I/II study of neoadjuvant combined chemotherapy plus tranilast for esophageal cancer was initiated and is currently under way (24).

In this study, we demonstrated, both *in vitro,* using co-culture models of NSCLC

cells with CAFs, and *in vivo*, that tranilast prevented the acquisition of resistance to molecular-targeted drugs by suppressing the IL-6/JAK/STAT3 signaling pathway and inhibition of EMT in cancer cells. IL-6 is one of the major cytokines released into the TME, which activates the cellular IL-6/JAK/STAT3 signaling pathway, promotes tumor cell proliferation and invasiveness, and inhibits cellular apoptosis (25). In addition, activation of the IL-6/STAT3 axis, both in an autocrine manner in oncogene-addicted cancer cells, and in a paracrine manner from CAFs, has been shown to contribute to the acquisition of treatment resistance (26,27). EMT refers to phenotypic conversion of cells from an epithelial type into a mesenchymal type, and confers the tumor metastatic behaviors of cancer cell invasion and migration on the tumor cells; it is also known to be another critical mechanism underlying the acquisition of CAF-mediated drug resistance (28). TGF-β is considered to be a key mediator of CAF-induced EMT. We demonstrated the inhibitory effect of tranilast on CAF-induced EMT, although the secretion of TGF-β from CAFs was not suppressed, unlike the case of IL-6 secretion from these cells (data not shown). Furthermore, TGF-β-induced EMT was also demonstrated to be suppressed by tranilast treatment. Considering these findings, tranilast appeared to have a direct effect of inhibiting EMT in the

cancer cells. Kang *et al.* showed that tranilast inhibited EMT by inhibiting the TGF-β/Smad pathway in peritoneal mesothelial cells (29); however, we could not confirm any changes in the Smad activity in our NSCLC cell lines (data not shown), suggesting that other signaling pathway(s) than the TGF-β/Smad may also be involved in the suppression of EMT by tranilast. Further studies are needed for a more precise elucidation of this intriguing biological mechanism.

In summary, we showed that tranilast inhibited CAF-mediated acquisition of resistance of NSCLC cells to molecular-targeted therapy via inhibiting the IL-6/STAT3 axis via its actions on the CAFs, and prevented EMT via its direct actions on the cancer cells. Based on these findings, we strongly suggest that combined administration of tranilast with molecular-targeted therapy is an attractive complementary therapeutic strategy to maximize the effect of molecular-targeted therapy.

Figures

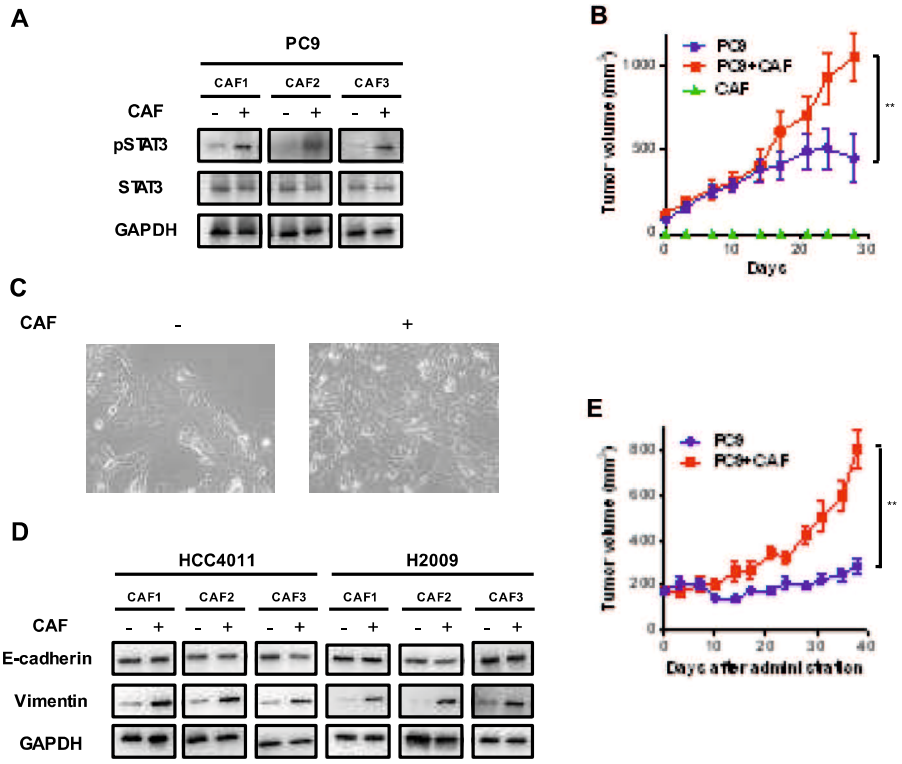

Figure 1. Effect of CAFs on the progression and acquisition of drug resistance of NSCLC through activation of STAT3 signaling and induction of EMT. A, PC9 cells were co-cultured with CAFs for 7 days, and the expression level of pSTAT3 was analyzed by Western blotting. B, PC9 cells alone, CAF1 cells alone, or PC9 cells plus CAF1 cells were subcutaneously implanted into the flanks of nude mice, and the tumor sizes were monitored. Each group consisted of 5 mice. Data shown are the means ± SE; **P<0.01. C, HCC4011 cells were co-cultured with CAFs, and morphological changes were observed. D, HCC4011 and H2009 cells were co-

cultured with CAFs for 72 hours, and the expression levels of EMT markers were analyzed by Western blotting. E, PC9 cells alone or PC9 cells plus CAF1 cells were subcutaneously implanted into the flanks of nude mice. When the tumors reached a diameter of approximately 150 mm3, the mice were treated with 5 mg/kg of osimertinib 5 times a week. The tumor volumes were then determined on the indicated days after the start of treatment. Each group consisted of 7 mice. Data shown are the means ± SE; **P<0.01.

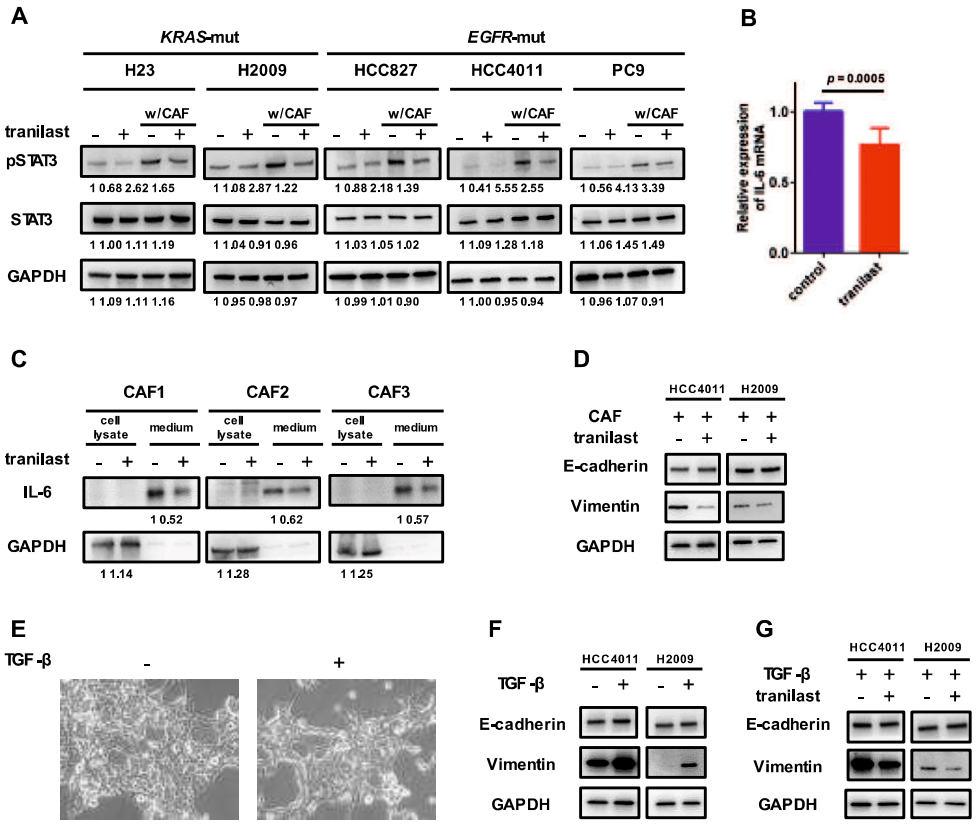

Figure 2. Inhibitory effect of tranilast on CAF-induced pSTAT3 upregulation and EMT in NSCLC cells. A, NSCLC cell lines were cultured in the presence of tranilast for 7 days, and the expression level of pSTAT3 was analyzed by Western blotting. B, After tranilast treatment for 48 hours, the mRNA expression levels of IL-6 in the CAFs were measured by real-time PCR. Each measurement was conducted in triplicate and the data are representative of three independent

experiments (mean ± SE) conducted using different CAF sublines (CAF1, CAF2, and CAF3). C, Secretion of IL-6 in the culture medium of the CAFs was assessed by Western blotting. D, NSCLC cell lines and CAFs were co-cultured in the presence of tranilast for 7 days, and the EMT status was analyzed by Western blotting. E, HCC4011 cells were treated with TGF-β, and morphological changes were observed. F, After TGF-β treatment for 72 hours, the EMT status in the HCC4011 and H2009 cells were analyzed. G, HCC4011 and H2009 cells were treated with TGF-β in the presence or absence of tranilast for 72 hours, and the EMT status was analyzed by Western blotting.

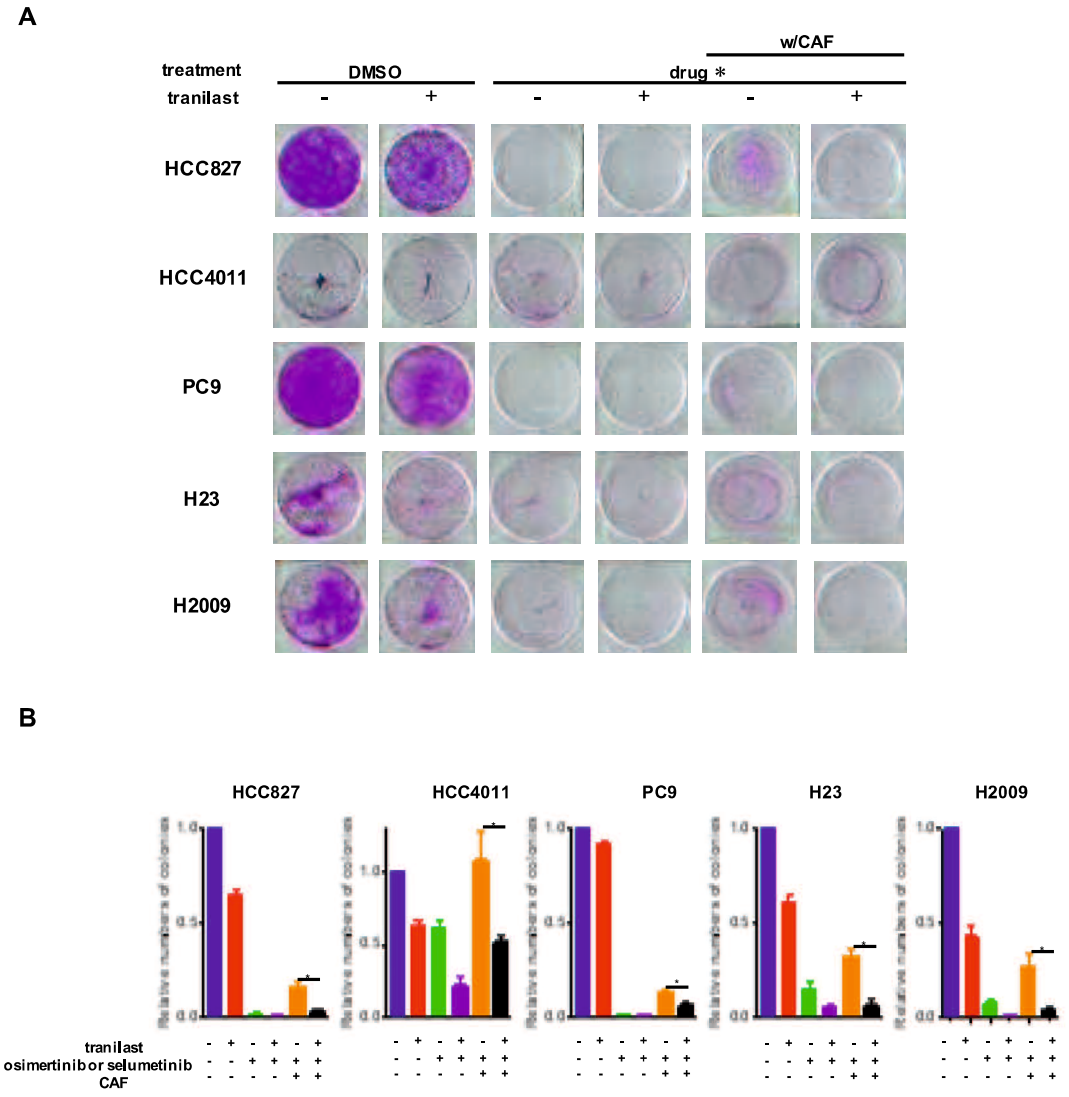

Figure 3. Effect of tranilast on CAF-induced drug resistance in NSCLC cells. A, NSCLC cell lines were cultured with or without CAFs in the presence or absence of tranilast for 7 days. B, The number of colonies was quantified using the ImageJ software. Each condition was assayed in duplicate and the data are representative of three independent experiments. *: osimertinib for HCC827,

HCC4011 and PC9 cells, and selumetinib for H23 and H2009 cells. Data shown are the means ± SE; *P<0.05, **P<0.01

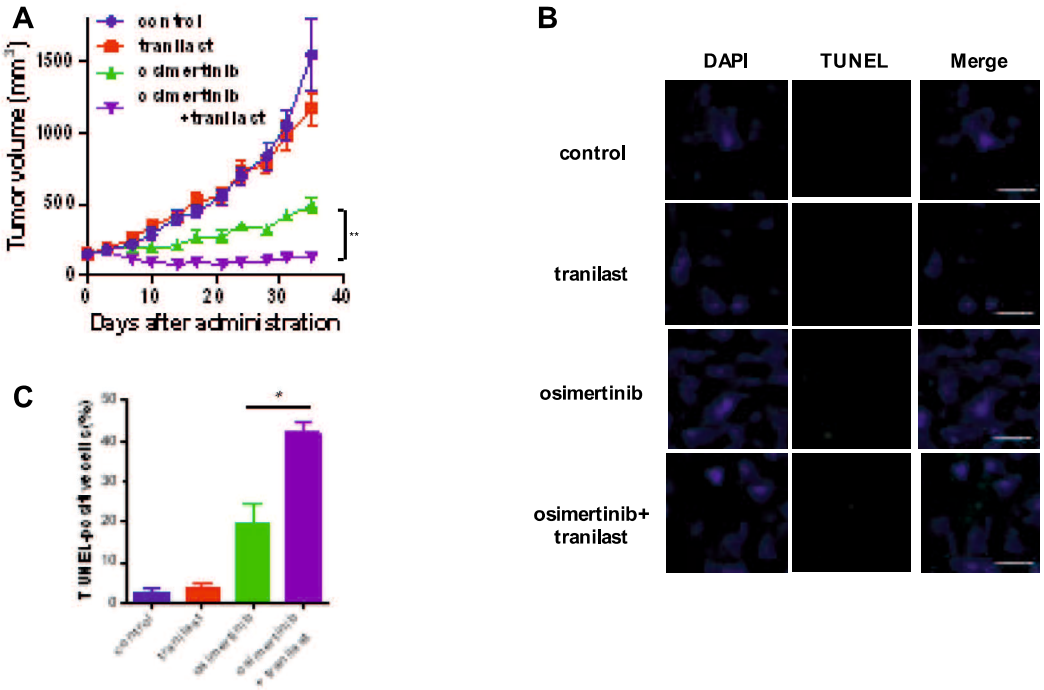

Figure 4. Enhancement of the tumor-inhibitory effect of tranilast in a mouse xenograft model of NSCLC cells plus CAFs. A, A mixture of PC9 cells and CAFs was subcutaneously implanted into the flanks of nude mice. The mice were treated with tranilast (200 mg/kg) alone, osimertinib (5 mg/kg) alone, or a combination of osimertinib plus tranilast by oral gavage five times a week. The tumor volumes were determined on the indicated days after the start of the treatments. Each group consisted of 7 mice. Data shown are the means ± SE; **P<0.01. B, TUNEL staining (green) and DAPI (blue) staining showing the apoptotic neuronal nuclei and all the cell nuclei under microscopy. Scale bars: 50

μm. C, The population of TUNEL-positive cells is shown as a percentage of the total number of cells. Data represent the means ± SE of five random fields. *P<0.05, vs. DAPI: 4′,6-Diamidino-2-phenylindole. TUNEL: terminal deoxynucleotidyl transferase dUTP nick-end labeling.

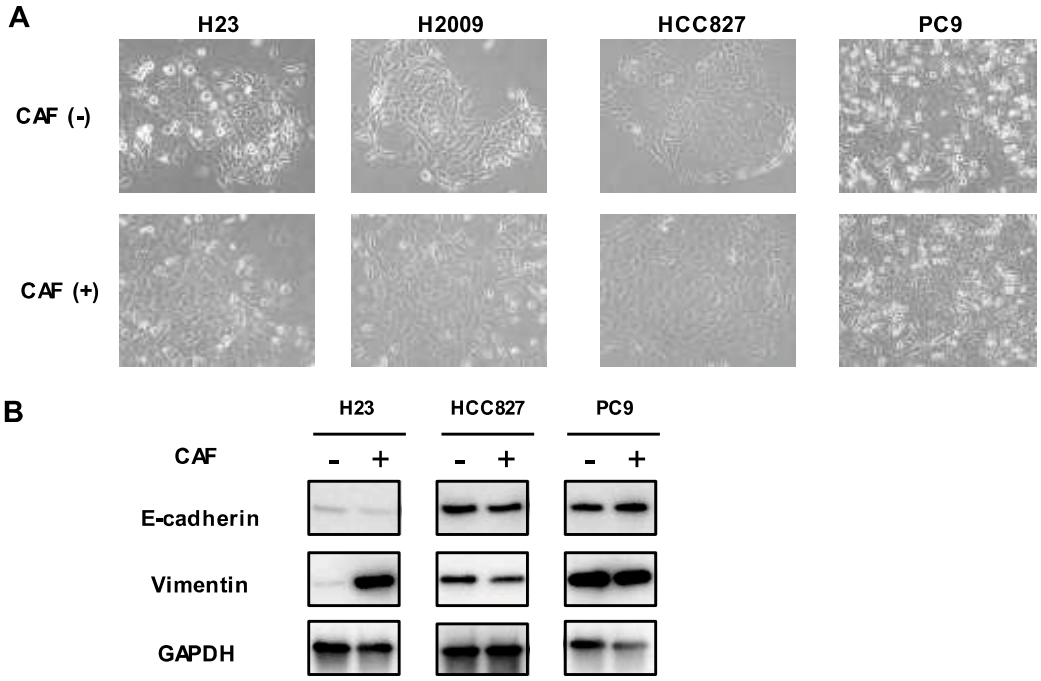

Fig. S1. Effect of CAF co-cultured to NSCLC cell lines. A, Morphological changes were not clear in 4 NSCLS cell lines. B, H23 cells showed upregulation of vimentin, but PC9 and HCC827 cells didn't show significant changes.

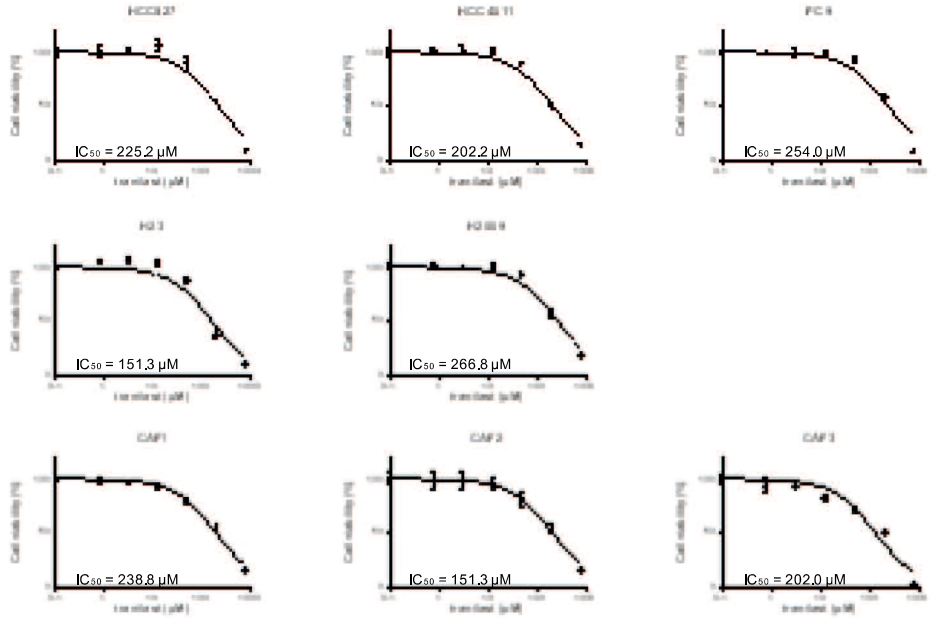

Fig. S2. IC50 value of tranilast for NSCLC cell lines and CAFs. Cells were treated with tranilast for 72 h. Cell viability was determined using CellTiter 96 Aqueous bromide dye. Each experiment was assayed in eight replicate determinations, and the data are representative of three independent experiments.

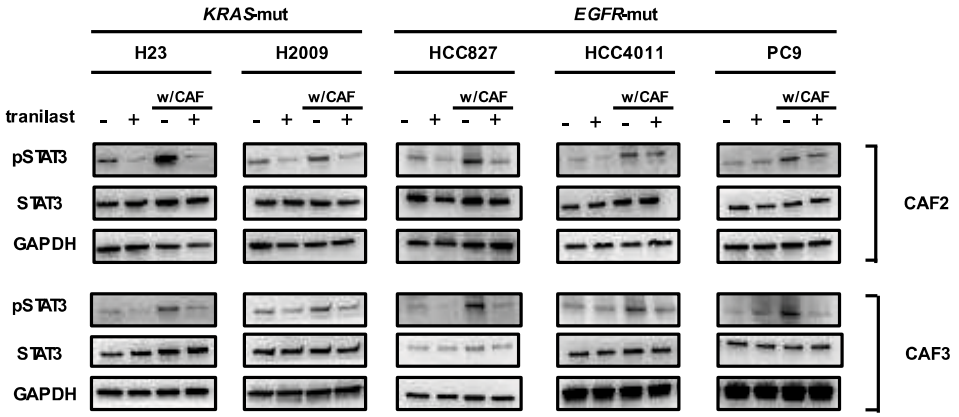

Fig. S3 Inhibitory effect of tranilast on CAF-induced pSTAT3 upregulation in NSCLC. NSCLC cell lines were co-cultured with tranilast for 7 days, and pSTAT3 was analyzed by Western blotting.

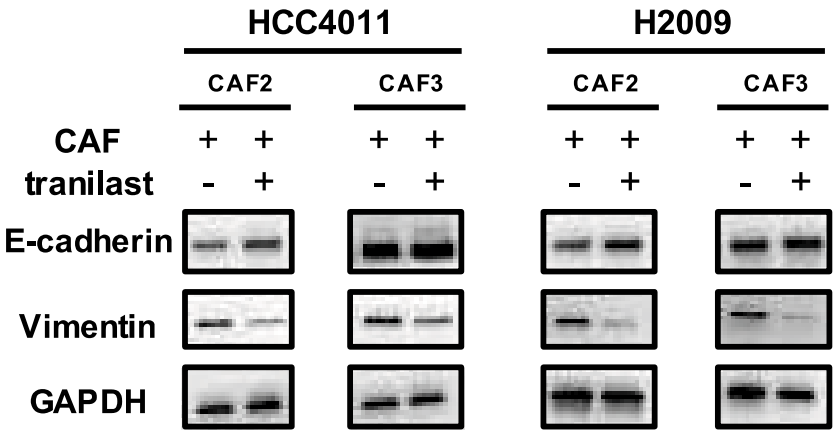

Fig. S4. Inhibitory effect of tranilast on CAF-induced EMT in NSCLC. NSCLC cell lines and CAFs were co-cultured with tranilast for 7 days, and EMT status was analyzed by Western blotting.

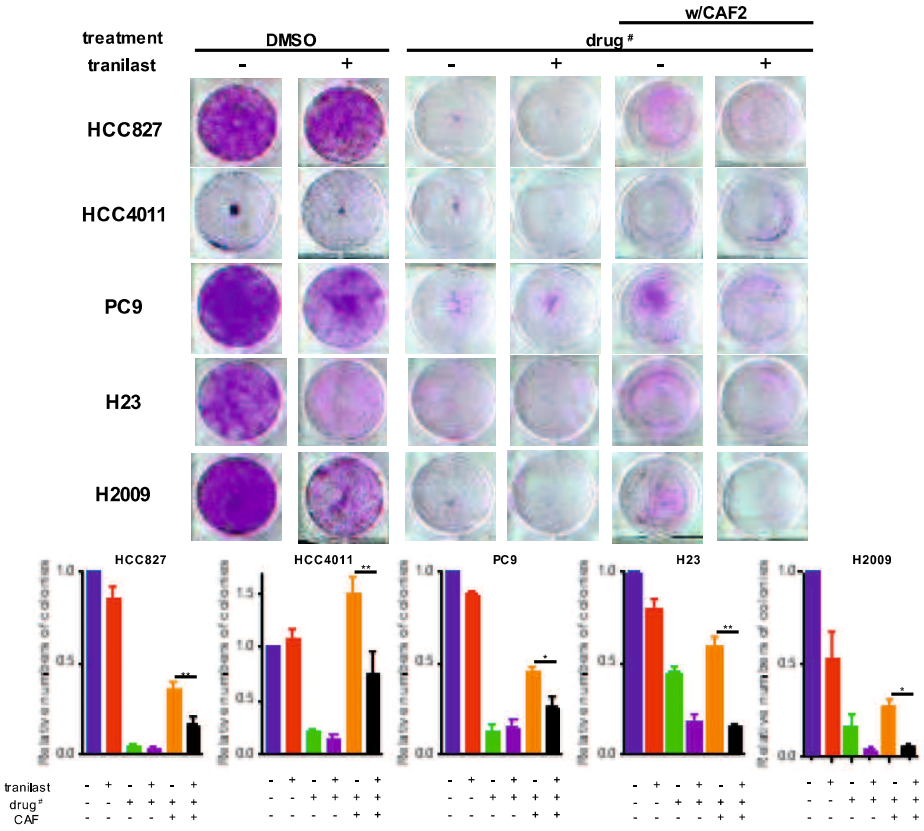

Fig. S5A Effect of tranilast on CAF2-induced drug resistance. NSCLC cell lines were cultured with or without CAF2 in the presence or absence of tranilast for 7 days. The number of colonies were measured using ImageJ. Each condition was assayed in duplicate determinations and data are representative of three independent experiments. # : osimertinib for HCC827, HCC4011 and PC9 cells, and selumetinib for H23 and H2009. Data are shown as mean ± SE; *P < 0.05, **P < 0.01

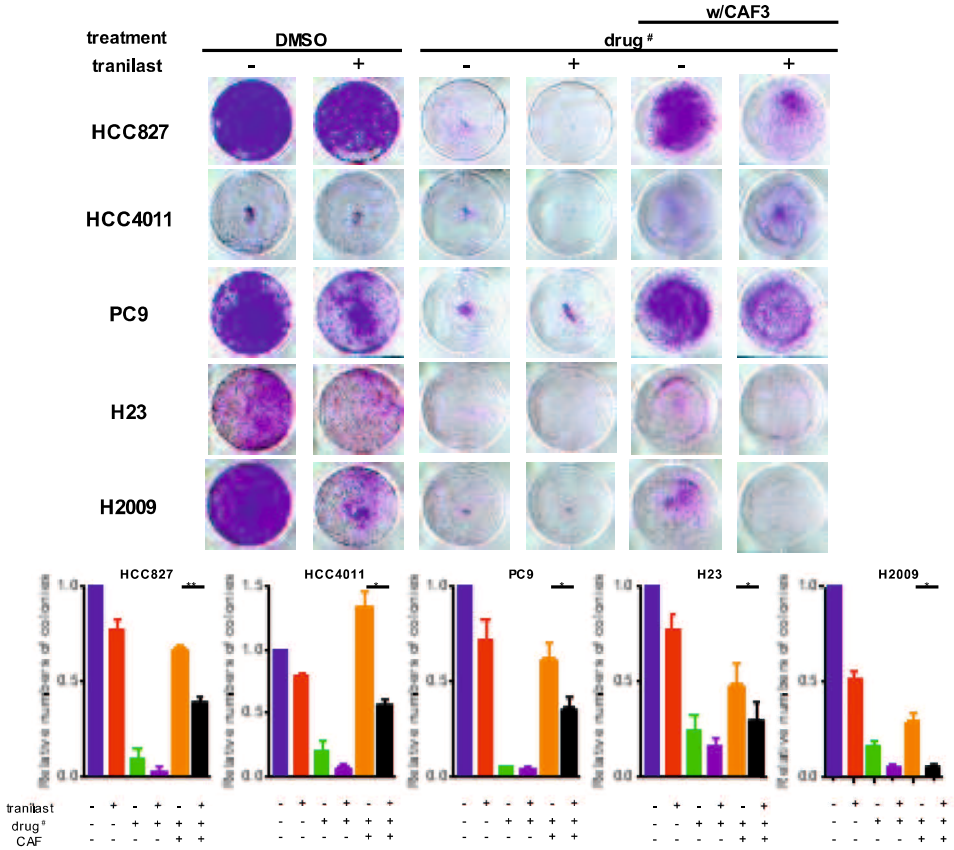

Fig. S5B Effect of tranilast on CAF3-induced drug resistance. NSCLC cell lines were cultured with or without CAF3 in the presence or absence of tranilast for 7 days. The number of colonies were measured using ImageJ. Each condition was assayed in duplicate determinations and data are representative of three independent experiments. # : osimertinib for HCC827, HCC4011 and PC9 cells, and selumetinib for H23 and H2009. Data are shown as mean ± SE; *P < 0.05, **P < 0.01

References

1. Bray F, Ferlay J, Soerjomataram I, Siegel RL, Torre LA, Jemal A. Global cancer statistics 2018: GLOBOCAN estimates of incidence and mortality worldwide for 36 cancers in 185 countries. CA Cancer J Clin **2018**;68(6):394-424 doi 10.3322/caac.21492.
2. Pao W, Girard N. New driver mutations in non-small-cell lung cancer. The Lancet Oncology **2011**;12(2):175-80 doi 10.1016/s1470-2045(10)70087-5.
3. Yu HA, Arcila ME, Rekhtman N, Sima CS, Zakowski MF, Pao W*, et al.* Analysis of tumor specimens at the time of acquired resistance to EGFR-TKI therapy in 155 patients with EGFR-mutant lung cancers. Clin Cancer Res **2013**;19(8):2240-7 doi 10.1158/1078-0432.CCR-12-2246.
4. Yu HA, Suzawa K, Jordan E, Zehir A, Ni A, Kim R*, et al.* Concurrent Alterations in EGFR-Mutant Lung Cancers Associated with Resistance to EGFR Kinase Inhibitors and Characterization of MTOR as a Mediator of Resistance. Clin Cancer Res **2018**;24(13):3108-18 doi 10.1158/1078-0432.CCR-17-2961.
5. Shien K, Papadimitrakopoulou VA, Ruder D, Behrens C, Shen L, Kalhor N*, et al.* JAK1/STAT3 Activation through a Proinflammatory Cytokine Pathway Leads to Resistance to Molecularly Targeted Therapy in Non-Small Cell Lung Cancer. Mol Cancer Ther **2017**;16(10):2234-45 doi 10.1158/1535-7163.MCT-17-0148.
6. Yu Y, Xiao CH, Tan LD, Wang QS, Li XQ, Feng YM. Cancer-associated fibroblasts induce epithelial-mesenchymal transition of breast cancer cells through paracrine TGF-beta signalling. Br J Cancer **2014**;110(3):724-32 doi 10.1038/bjc.2013.768.
7. Gao Q, Yang Z, Xu S, Li X, Yang X, Jin P*, et al.* Heterotypic CAF-tumor spheroids promote early peritoneal metastatis of ovarian cancer. J Exp Med **2019**;216(3):688-703 doi 10.1084/jem.20180765.
8. Karagiannis GS, Poutahidis T, Erdman SE, Kirsch R, Riddell RH, Diamandis EP. Cancer-associated fibroblasts drive the progression of metastasis through both paracrine and mechanical pressure on cancer tissue. Mol Cancer Res **2012**;10(11):1403-18 doi 10.1158/1541-7786.MCR-12-0307.
9. Masuda T, Tsuruda Y, Matsumoto Y, Uchida H, Nakayama KI, Mimori K. Drug repositioning in cancer: The current situation in Japan. Cancer Sci **2020**;111(4):1039-46 doi 10.1111/cas.14318.
10. Komtsu H, Kojima M, Tsutsumi N, Hamano S, Kusama H, Ujiie A*, et al.* Study of the mechanism of inhibitory action of tranilast on chemical mediator release. Jpn J Pharmacol **1988**;46:43-51.
11. Suzawa H, Kikuchi S, Arai N, Koda A. The mechanism involved in the inhibitory action of

tranilast on collagen biosynthesis of keloid fibroblasts. Japan J Pharmacol **1992**;60:91-6.

12. Hiraide S, Yanagawa Y, Iizuka K. Tranilast inhibits interleukin-33 production by macrophages. Eur J Pharmacol **2018**;818:235-40 doi 10.1016/j.ejphar.2017.10.057.
13. Hinshaw DC, Shevde LA. The Tumor Microenvironment Innately Modulates Cancer Progression. Cancer Res **2019**;79(18):4557-66 doi 10.1158/0008-5472.CAN-18-3962.
14. Sahai E, Astsaturov I, Cukierman E, DeNardo DG, Egeblad M, Evans RM*, et al.* A framework for advancing our understanding of cancer-associated fibroblasts. Nat Rev Cancer **2020**;20(3):174-86 doi 10.1038/s41568-019-0238-1.
15. Azuma H, Banno K, Yoshimura T. Pharmacological properties of N-(3',4'-dimethoxycinnamoyl) anthranilic acid (N-5'), a new anti-atopic agent. Br J Pharmacol **1976**;58:483-8.
16. Isaji M, Nakajoh M, Naito J. Selective inhibition of collagen accumulation by N-(3, 4-dimethoxycinnamoyl)anthranilic acid (N-5') in granulation tissue. Biochem Pharmacol **1987**;36:469-74.
17. Isaji M, Miyata H, Ajisawa Y, Takehara Y, Yoshimura N. Tranilast inhibits the proliferation, chemotaxis and tube formation of human microvascular endothelial cells in vitro and angiogenesis in vivo. Br J Pharmacol **1997**;122:1061-6.
18. Darakhshan S, Ghanbari A. Tranilast enhances the anti-tumor effects of tamoxifen on human breast cancer cells in vitro. J Biomed Sci **2013**;20.
19. Prud'homme GJ, Glinka Y, Toulina A, Ace O, Subramaniam V, Jothy S. Breast cancer stem-like cells are inhibited by a non-toxic aryl hydrocarbon receptor agonist. PLoS One **2010**;5(11):e13831 doi 10.1371/journal.pone.0013831.
20. Saito H, Fushida S, Harada S, Miyashita T, Oyama K, Yamaguchi T*, et al.* Importance of human peritoneal mesothelial cells in the progression, fibrosis, and control of gastric cancer: inhibition of growth and fibrosis by tranilast. Gastric Cancer **2018**;21(1):55-67 doi 10.1007/s10120-017-0726-5.
21. Hiroi M, Onda M, Uchida E, Aimoto T. Anti-tumor Effect of N-[3,4-dimethoxycinnamoyl]-anthranilic Acid (tranilast) on Experimental Pancreatic Cancer. Journal of Nippon Medical School **2002**;69:224-34.
22. Shiozaki A, Kudou M, Ichikawa D, Fujiwara H, Shimizu H, Ishimoto T*, et al.* Esophageal cancer stem cells are suppressed by tranilast, a TRPV2 channel inhibitor. J Gastroenterol **2018**;53(2):197-207 doi 10.1007/s00535-017-1338-x.
23. Darakhshan S, BidmeshkiPour A. Tranilast: A review of its therapeutic applications. Pharmacological Research **2014**;91:15-28.
24. Shiozaki A, Kudou M, Fujiwara H, Konishi H, Shimizu H, Arita T*, et al.* Clinical safety and efficacy of neoadjuvant combination chemotherapy of tranilast in advanced esophageal

squamous cell carcinoma: Phase I/II study (TNAC). Medicine (Baltimore) **2020**;99(50):e23633 doi 10.1097/MD.0000000000023633.

25. Lederle W, Depner S, Schnur S, Obermueller E, Catone N, Just A*, et al.* IL-6 promotes malignant growth of skin SCCs by regulating a network of autocrine and paracrine cytokines. Int J Cancer **2011**;128(12):2803-14 doi 10.1002/ijc.25621.
26. Lee HJ, Zhuang G, Cao Y, Du P, Kim HJ, Settleman J. Drug resistance via feedback activation of Stat3 in oncogene-addicted cancer cells. Cancer Cell **2014**;26(2):207-21 doi 10.1016/j.ccr.2014.05.019.
27. Karakasheva TA, Lin EW, Tang Q, Qiao E, Waldron TJ, Soni M*, et al.* IL-6 Mediates Cross-Talk between Tumor Cells and Activated Fibroblasts in the Tumor Microenvironment. Cancer Res **2018**;78(17):4957-70 doi 10.1158/0008-5472.CAN-17-2268.
28. Lamouille S, Xu J, Derynck R. Molecular mechanisms of epithelial-mesenchymal transition. Nat Rev Mol Cell Biol **2014**;15(3):178-96 doi 10.1038/nrm3758.
29. Kang SH, Kim SW, Kim KJ, Cho KH, Park JW, Kim CD*, et al.* Effects of tranilast on the epithelial-to-mesenchymal transition in peritoneal mesothelial cells. Kidney Res Clin Pract **2019** doi 10.23876/j.krcp.19.049.

GENERAL CONCLUSION

This study investigated the novel anti-tumour effects of existing drugs utilising drug repositioning.

The study of chapter 1 confirmed that monensin, which is used in veterinary medicine, has an inhibitory effect on EMT in an in vitro experimental system. *In silico* analysis showed that monensin was expected to have an anti-tumour effect, which was demonstrated in an actual *in vitro* experiment. The current study demonstrated the possible utility of monensin as a prophylactic when co-administered with antitumor reagents to prevent the acquisition of an EMT signature, thereby prolonging the disease-control period.

In chapter 2, we showed that tranilast inhibited CAF-mediated acquisition of resistance of NSCLC cells to molecular-targeted therapy via inhibiting the IL-6/STAT3 axis via its actions on the CAFs, and prevented EMT via its direct actions on the cancer cells. Based on these findings, we strongly suggest that combined administration of tranilast with molecular-targeted therapy is an attractive complementary therapeutic strategy to maximize the effect of molecular-targeted therapy.

These two experiments were conducted using drug repositioning. Drug

repositioning is currently being introduced as a means of breaking the stagnation in new drug development. It is expected that future drugs will be developed more speedily by using drug repositioning. We expect this research to contribute to the development of novel cancer therapies.